

Journal Pre-proofs

Research papers

oSpatio-temporal sensitivity analysis of the wetland modules of a semi-distributed hydrological model

Marianne Blanchette, Étienne Foulon, Alain N. Rousseau

PII: S0022-1694(23)00725-4

DOI: <https://doi.org/10.1016/j.jhydrol.2023.129783>

Reference: HYDROL 129783

To appear in: *Journal of Hydrology*

Received Date: 18 January 2023

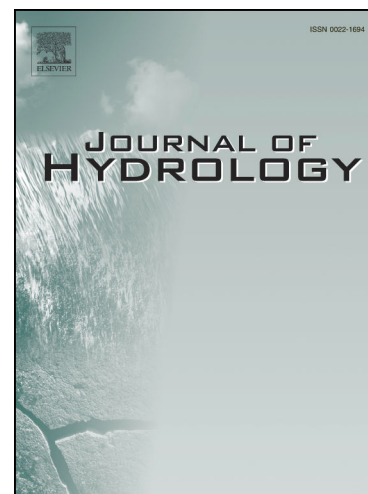
Revised Date: 9 April 2023

Accepted Date: 5 June 2023

Please cite this article as: Blanchette, M., Foulon, E., Rousseau, A.N., oSpatio-temporal sensitivity analysis of the wetland modules of a semi-distributed hydrological model, *Journal of Hydrology* (2023), doi: <https://doi.org/10.1016/j.jhydrol.2023.129783>

This is a PDF file of an article that has undergone enhancements after acceptance, such as the addition of a cover page and metadata, and formatting for readability, but it is not yet the definitive version of record. This version will undergo additional copyediting, typesetting and review before it is published in its final form, but we are providing this version to give early visibility of the article. Please note that, during the production process, errors may be discovered which could affect the content, and all legal disclaimers that apply to the journal pertain.

© 2023 Elsevier B.V. All rights reserved.



1 **Spatio-temporal sensitivity analysis of the wetland modules of a semi-distributed**
2 **hydrological model**

3 Marianne Blanchette^{a*} (marianne.blanchette@inrs.ca)

4 Étienne Foulon^a (etienne.foulon@inrs.ca)

5 Alain N. Rousseau^a (alain.rousseau@inrs.ca)

6

7

8 ^aINRS-ETE / Institut National de la Recherche Scientifique – Eau Terre Environnement, 490 rue
9 de la Couronne, G1K 9A9, Quebec City, Québec, Canada

10 *corresponding author

11 Abstract

12 Hydrological models offer the opportunity to evaluate wetland conservation networks as nature-
13 based solutions to mitigate hydrological extremes. To optimize the replication of a hydrological
14 model response (i.e., stream flows), the models rely on input data (land cover, hydrographic
15 network, soil types, topography, meteorological data) and parameters. However, the effect of
16 parametric uncertainty on the simulated variables and the spatio-temporal variability of this
17 sensitivity are insufficiently documented. This study presents an application of the novel global
18 sensitivity analysis method, the Variogram Analysis of Response Surface, to the isolated and
19 riparian wetland modules of HYDROTEL, a semi-distributed, process-based, deterministic model,
20 on two watersheds located in the province of Quebec, Canada. The analysis accounted for: (i) the
21 spatial variability by assessing the sensitivity at various locations in the watersheds and by
22 compiling sensitivity indices for wetland networks discretized following the Strahler order
23 classification which quantifies the structure of hydrographic networks and (ii) the temporal
24 variability of the sensitivity using the Generalized Global Sensitivity Matrix. The results indicate
25 that the parameters defining the geometry of wetlands (area, depth) are the most sensitive for
26 both isolated and riparian wetlands, and for all Strahler orders. The temporal assessment of
27 sensitivity highlights the seasonal controlling processes, including a peaking sensitivity of the
28 maximum water depth in wetlands during spring snowmelt, whereas the sensitivity of the
29 evapotranspiration parameter increases during summer, but is null during winter. Results also
30 indicate that the parameters of the isolated modules are more sensitive for wetlands located on
31 lower stream order (upstream/headwaters) while those of the riparian modules display a greater
32 sensitivity when wetlands are located on higher Strahler orders (downstream/main channel).
33 These findings deepen our understanding of the impact of wetland features on stream flows and
34 provide guidelines to plan future data acquisition campaigns in wetlandscapes.

35

36 Keywords

37 HYDROTEL, hydroconnectivity, time-varying sensitivity analysis, Variogram Analysis of Response
38 Surface, field data acquisition, Strahler order

39 1. Introduction

40 The development of hydrological models has advanced our understanding of how landscape
41 features affect watershed hydrology. For example, the integration of wetland hydrology in
42 watershed-scale models has allowed researchers to investigate how river flows react to diverse
43 configurations of wetland coverage, location, typologies, and/or hydro-connectivity in various
44 climates and geological environments (Blanchette et al., 2022; Evenson et al., 2018; Fossey et
45 al., 2016; Goyette et al., 2022). Over the last decade or so, wetlands have been the subject of
46 increasing scientific and political attention, thanks to their key role in mitigating stream flows.
47 Nevertheless, it is essential to remain critical when drawing conclusions from model outputs.
48 Indeed, exhaustive sensitivity and uncertainty analyses of semi-distributed hydrological models
49 used to assess the impact of wetlands on hydrological variables have yet to be carried out
50 comprehensively. Consequently, although models were developed with the most up-to-date
51 scientific knowledge of wetland hydrology, it is still unclear how uncertainties in input data and
52 model parameters may affect simulation results. For instance, most semi-distributed hydrological
53 models rely on empirical power equations describing volume-area-depth relationships that are
54 governed by wetland geometry (Rahman et al., 2016). Among models, HYDROTEL, a semi-
55 distributed hydrological model (Fossey et al., 2015) assumes that maximum wetland extents can
56 be derived from remotely sensed land cover data. This maximum surface area, along with
57 parameters of the volume-area-depth relationships, subsequently intervene at every
58 computational time step to assess water storage and fluxes. Meanwhile, remotely-sensed data
59 are affected by antecedent meteorological and soil moisture conditions at the time of acquisition
60 – and conversely govern the spatial resolution of input data and wetland parameters; thus,
61 impacting model response. All these issues emphasize the need for an in-depth quantification of
62 the effect of any parameter-induced uncertainties on model outputs.

63 By definition, sensitivity analysis (SA) “studies how the uncertainty in the output of a model can
64 be apportioned to the different sources of uncertainty in the model input” (Saltelli et al., 2004). The
65 scientific community agrees that SA should be the first step of any new model implementation, as
66 it provides key insights on its performances to reproduce a given system. Razavi et al. (2021)
67 reported four overarching purposes of SA: (i) explore causalities, processes, and interactions of
68 the modelled system, (ii) reduce dimensionality, (iii) target data acquisition, and (iv) support
69 decision. Two main categories of SA coexist. First, local SA refers to methods where inputs are
70 modified around a nominal value to observe the effect on model response. Local methods provide
71 a simple and fast option to perform SA, but they are limited to assessing the impact of individual
72 parameters independently, not accounting for possible interactions. In this context, local methods
73 are inadequate when it comes to assessing complex models representing Earth and
74 environmental systems, including hydrological models. For these systems, global sensitivity
75 analysis (GSA) methods, such as derivative-based (Morris, 1991), distribution-based (Sobol,
76 1993), variogram-based (Razavi and Gupta, 2016a; Razavi and Gupta, 2016b), or regression-
77 based (Iman and Helton, 1988), are better suited as they “provide a ‘global’ representation of how
78 the different factors work and interact across the full problem space to influence some function of
79 the system output” (Razavi et al., 2021). Although it comes with high computational costs, GSA
80 remains a judicious means of comprehensively assessing the quality of model input approximation
81 and diagnosing any flaw in model structure.

82 Traditional sensitivity analysis applications rely on performance metrics, which aggregate the
83 propagation of uncertainties and may lead to a loss of information regarding sensitivity at finer
84 temporal scales (Pianosi and Wagener, 2016). In response to this loss of information, time-variant
85 GSA tools, where sensitivity metrics are computed at every time step, have been developed to
86 study how simulated processes dominance varies in time (Pianosi and Wagener, 2016; Razavi

87 and Gupta, 2019). Among others (Bajracharya et al., 2020; Korgaonkar et al., 2020; Medina and
88 Muñoz, 2020; Razavi and Gupta, 2019), Pianosi and Wagener (2016) performed a time-variant
89 sensitivity analysis using PAWN (Pianosi and Wagener, 2015), a density-based SA method, on
90 the Hydrologiska Byråns Vattenbalansavdelning (HBV) model applied to three watersheds in the
91 USA: the English River in Iowa, the French Broad River in North Carolina, and the Guadalupe
92 River in Texas. Their results confirmed that time-variant sensitivity analysis can reveal sensitivity
93 information that could be hidden in SA based on aggregated performance metrics.

94 Among the models that are well suited for representing wetlands at the watershed scale, many
95 underwent a form of SA. While developing a SWAT extension module simulating riparian wetlands
96 (RW), Liu et al. (2008) conducted a partial and local SA on the wetland geometric parameters
97 (normal depth and ratio between normal and maximum surface areas) relative to stream flow. For
98 an application on the Upper Canagagigue Creek watershed (53 km²) in Southern Ontario, Canada,
99 their results highlighted the necessity of calibrating geometric parameters, especially when field
100 data are available. Building upon this work, Rahman et al. (2016) modified the RW extension
101 module of SWAT by replacing the unidirectional interaction between wetlands and river/aquifer
102 with a hydraulic-based bidirectional connection. To assess how these parameters affect the
103 sensitivity of stream flows and wetland storage, they analyzed the temporal dynamics of parameter
104 sensitivity (Reusser et al., 2011), based on the Fourier amplitude sensitivity test (FAST; Cukier et
105 al., 1973). They applied this method on two sub-basins (wetland drainage area > 96%) located in
106 the Barak-Kushiyara River transboundary watershed (35,563 km²), shared by India and
107 Bangladesh. Their results revealed a high temporal variability in parameter sensitivity. To assess
108 the impact of geographically isolated wetlands (IWs) on water table and base flow variation,
109 McLaughlin et al. (2014) combined shallow-water table and soil moisture process-based models
110 with a wetland hydrology model. Their SA showed that wetland elevation and confining layer
111 elevation, which are driven by changes in the geometry of the wetland system, displayed a
112 significant sensitivity. As a first attempt to understand the relative sensitivities of the wetland
113 parameters of HYDROTEL, a semi-distributed hydrological model, Fossey et al. (2015) performed
114 a local SA using the Bécancour River watershed (2,597 km², 12% of wetlands cover, including, 8
115 % of IWs and 4 % of RWs). They used the local one-parameter-at-a-time method (Ben Nasr, 2014;
116 Bouda et al., 2014; Mailhot and Villeneuve, 2003) to evaluate how parameter variations affected
117 stream flows at three different locations within the watershed (following an upstream-downstream
118 gradient). Their results suggested that the parameters of the IW module are the most influential
119 ones when compared to those of the RW module, with some variability between the river reaches
120 of interest. Although quite informative, some questions have remained, especially regarding
121 interactions between parameters and large parameter space. More importantly, their investigation
122 raises questions regarding the spatio-temporal variability of sensitivity, including: (i) Are stream
123 flows equally sensitive to various wetland spatial configurations at the watershed scale? (ii) How
124 does sensitivity temporally vary? One way to provide answers to these questions is to perform a
125 spatio-temporal GSA. This would not only provide a more comprehensive understanding of the
126 influence of the wetland parameters of HYDROTEL, but also help us to interpret the modelling
127 results; in this instance to put in perspective the role of wetlands at the watershed scale. This
128 would be particularly relevant given the fact that the model has been used to assess the role of
129 wetlands: (i) during floods in the large Canada-USA Lake Champlain Richelieu River watershed
130 (Rousseau et al., 2022); (ii) as flood resilience landscapes in China (Wu et al., 2020b), (iii) in
131 regulating streamflows (Wu et al., 2020a), and (iv) the effect of river damming on their hydrological
132 functions (Wu et al., 2021). The model has also been used to investigate whether wetlands can
133 mitigate the impact of climate change in both Canada (Fossey and Rousseau, 2016a; Fossey and
134 Rousseau, 2016b) and China (Wu et al., 2022).

135 In this paper, we present the results of a GSA on the IW and RW modules of HYDROTEL, using
136 a novel variogram-based method (Razavi and Gupta, 2016a; Razavi and Gupta, 2016b). We
137 combine this algorithm with the Generalized Global Sensitivity Matrix (GGSM) to account for the
138 sensitivity temporal variability. We also specifically address the spatial variability by: (i) carrying
139 out the SA on two distinct watersheds located in southeastern Canada, the St. Charles River and
140 the Bécancour River watersheds, and (ii) assessing the sensitivity at various locations in the latter
141 watersheds. Moreover, for both watersheds, we test how different spatial configurations of
142 wetlands at the watershed scale can affect parameter sensitivity.

143 **2. Material and methods**

144 **2.1. Study area**

145 Two watersheds with distinct characteristics of wetland cover, land use, and soils, were selected
146 to perform the SA: the St. Charles River watershed (554 km²) and the Bécancour River watershed
147 (2,597 km²), both located in Quebec, Canada (Fig. 1). The St. Charles River watershed comprises
148 five tributaries with a stream network ranging from 1 to 5 Strahler orders: Des Hurons (137 km²),
149 Jaune (82 km²), Nelson (74 km²), Lorette (72 km²) and Du Berger (57 km²). The watershed is
150 located on the North shore of the St. Lawrence River. Many lakes are found in the watershed, the
151 most important being Lake St. Charles which is used as a drinking water reservoir for more than
152 300,000 citizens of the region. To ensure long-term protection of the water quality and quantity,
153 Quebec City recently acquired a bio-hydrologically relevant wetland complex to help mitigate the
154 impact of accelerated anthropogenic development in some parts of the watershed. In this specific
155 watershed, there is indeed good synergy between wetland scientists and municipal authorities to
156 improve our understanding of wetland services and used them in urban planning. Wetlands and
157 their contributing areas (CA) cover 6% and 22% of the watershed, respectively. The Nelson sub-
158 watershed (Fig. 2 (d); 9%) has the highest wetland cover, followed by the Lorette sub-watershed
159 (Fig. 2 (g); 7%). While those two sub-watersheds are dominated by IWs, RWs dominate the other
160 sub-watersheds while, the majority of IWs are found in headwater hillslopes. The watershed is
161 mostly urbanized in the downstream part (southern portion), while the northern portion is mainly
162 covered with forests belonging to the balsam fir-yellow birch and balsam fir-white birch bioclimatic
163 region (Agence des forêts privées du Québec 03, 2001). The watershed is characterized by
164 subpolar temperatures, humid precipitation, and mean growing season in the north, and by
165 moderate temperatures, sub-humid precipitation, and long growing season in the southern part
166 (Fig. 3 (a, top and middle); Gerardin and McKenney, 2001; Litynski, 1988). The Köppen-Geiger
167 climate classification places the watershed in the warm-summer humid continental climate (Dfb).
168 However, this classification could evolve to a hot-summer humid continental climate (Dfa) over
169 the 2071-2100 horizon (Beck et al., 2018). Based on 47 climate change projections, mean daily
170 temperatures are expected to increase between current (1980-2019) and future (2060-2099)
171 climate, and the snow:rain precipitation ratio will also decrease during winter and early spring for
172 the St. Charles watershed specifically (Goyette et al., 2022). Covered with sandy loam, clay loam
173 and loamy sand soil textures, most of the watershed unfolds on the Grenville geological province,
174 but some parts of the downstream region are located within the St. Lawrence platform and the
175 Appalachians geological province. The conjunction of these three geological provinces and their
176 fault line explains a rather complex topography. It is characterized by rounded and crystalline hills
177 on the Grenville province with slopes up to 60%, smaller monticules and terraces in the central
178 part with slopes lower than 10%, and the part located on the Appalachian province consists of a
179 hill with slopes from 11 to 15% (Brodeur et al., 2009).

180 The Bécancour River starts at the outlet of Lake Bécancour, which is in the city of Thetford Mines,
181 and ends on the southern shore of the St. Lawrence River, close to the City of Bécancour. The

182 watershed has a rather high wetland cover (12%), draining 31 % of its territory (Fig. 2). Forested
 183 peatlands (4.9%) and swamps (4.0%) dominate (Canards Illimités Canada and Ministère de
 184 l'Environnement et Lutte contre les changements climatiques, 2020), but this watershed also has
 185 an important cover of open ombrotrophic peatlands (1.1%). The hydrographic network includes
 186 62 lakes (> 1 ha) and drains a territory that is mostly covered by forests (54%, eastern sugar
 187 maple-basswood and sugar maple-yellow birch bioclimatic domains; Agence Forestière des Bois-
 188 Francs 2015) and agriculture (23%). The watershed has moderate temperatures, sub-humid
 189 precipitations and a long growing season (Fig. 3 (b, top and middle); Gerardin and McKenney,
 190 2001; Litynski, 1988). Under current climate conditions, mean precipitation is 1,297 mm in the
 191 upper part and 1,085 mm at the outlet, while mean temperatures are 4 °C and 4.7 °C, at Thetford
 192 Mines (1971-2000) and Bécancour, respectively (Morin and Boulanger, 2005). Beck et al. (2018)
 193 predicted that the Köppen-Geiger climate classification will evolve from warm-summer humid
 194 continental to hot-summer humid continental in the future. Rugged landforms, strong slopes and
 195 altitude ranging between 100 and 600 m characterize the upper (southern) half of the watershed,
 196 located within the Appalachians Mountains, while the lower (northern) half extends on the St.
 197 Lawrence platform, where the topography is lightly undulated with gentler slopes and altitudes
 198 below 100 m. The surface deposits are characterized as till with a loamy soil texture in the upper
 199 part, while loamy sands cover the lower part. Since the majority of wetlands on the watershed are
 200 located in this region and to increase computational efficiency, the SA was performed upstream
 201 of hydrometric station 024014.

202 Considering their specific discharge (discharge divided by the total surface area of the watershed)
 203 the St. Charles and Bécancour River watersheds have similar hydrographs (Fig. 3. a and b,
 204 bottom). However, the St. Charles River watershed, which has a smaller area, a steeper
 205 topography, and slightly higher mean precipitations, shows more reactivity than the Bécancour
 206 watershed, including a higher spring snowmelt stream flow.

207 **Fig. 1. Location and Strahler order of wetlands on the (a) St. Charles River watershed and (b) the**
 208 **Bécancour River watershed.**

209 **Fig. 2. Total wetland (HEW) area and contributing area (CA) for each watershed and sub-watershed,**
 210 **presented by Strahler order. A stands for “all wetlands”.**

211 **Fig. 3. Hydrometeorological conditions over the 2000-2020 period of the (a) St. Charles and (b)**
 212 **Bécancour watersheds. The top figures present the minimum, mean, and maximum**
 213 **temperatures. The middle figures present minimum, mean, and maximum**
 214 **cumulatives of snow (P_s), rain (P_r), and total precipitation (P_{tot}). The bottom figures**
 215 **present the minimum, mean, and maximum specific discharge hydrographs from**
 216 **simulated streamflows.**

217 **2.2. PHYSITEL/HYDROTEL modelling platform, input data, processing steps and**

218 **wetland integration**

219 We performed a SA on the IW and RW modules of the PHYSITEL/HYDROTEL modelling platform,
 220 which is used by multiple institutions (Hydro-Québec, Yukon Energy) and universities (École de
 221 Technologies Supérieures, Université de Sherbrooke, Université Laval, Universidad Veracruzana
 222 in Mexico, Northeast Institute of Geography and Agroecology in China, to mention a few). These
 223 different applications of the model have confirmed its ability to reproduce accurately stream flows
 224 in a variety of hydroclimatic and geological contexts. In Quebec, specifically, HYDROTEL is used
 225 by the Water Expertise Division of the ministry of Environment, fight against Climate Change,
 226 Fauna and Park to simulate the flows of the provincial Hydroclimatic Atlas

227 (<https://cehq.gouv.qc.ca/atlas-hydroclimatique>). Using HYDROTEL in this study was also
 228 motivated by the availability of local expertise to analyze and interpret the results.

229 This platform includes a specialized geographic information system (GIS), PHYSITEL (Noël et al.,
 230 2014; Rousseau et al., 2011; Turcotte et al., 2001), which is used to build and format a
 231 physiographic database to support the implementation of distributed hydrological models.
 232 HYDROTEL (Bouda et al., 2014; Bouda et al., 2012; Fortin et al., 2001; Turcotte et al., 2007;
 233 Turcotte et al., 2003) is a semi-distributed, process-based, deterministic model, built around nine
 234 computational modules simulating different components of the hydrological cycle. Among them,
 235 meteorological data interpolation, snow accumulation and melt, soil temperature and freezing,
 236 potential evapotranspiration, and vertical water budget are applied at the relatively hydrologically
 237 homogeneous units (RHHUs, i.e., hillslopes) scale, the computational unit of HYDROTEL. Runoff
 238 routing relies on a geomorphological unit hydrograph (generated with a reference depth of water),
 239 which performs a temporal distribution of the vertical water budget output. Finally, water routing in
 240 the hydrographic network is computed at the river reach scale using as inputs water from the
 241 upstream river reach and runoff from the adjacent hillslopes. The model accounts for the
 242 contribution of wetlands to watershed hydrology *via* two wetland modules (representing IWs and
 243 RWs) integrated at the hillslope scale by Fossey et al. (2015). The IW module is represented as
 244 a control volume of the vertical water budget with its outlet connected to the runoff routing module.
 245 The RW module is partially integrated to the vertical water budget and has a connection to the
 246 river flow routing module.

247 For the St. Charles River watershed, a 20-m digital elevation model (DEM) and a vectorial river
 248 network (1:50,000), both extracted from Geogratis (Natural Resources Canada, 2013;
 249 <https://maps.canada.ca/czs/index-en.html>) were used. A 20-m resolution land cover map was
 250 built by combining various datasets (Blanchette et al., 2022) and the soil textures were extracted
 251 from the soil landscapes of Canada (Soil Landscapes of Canada Working Group, 2010). For the
 252 Bécancour River watershed, we used a previous implementation of the watershed (Fossey et al.,
 253 2016), which included: (i) a 30-m DEM from the Quebec Topographic Database, (ii) a vectorial
 254 river network provided by the Quebec Hydrological Expertise Center (*Centre d'expertise hydrique
 255 du Québec*, CEHQ), (iii) a 30-m resolution land cover map of 2012 provided by University of
 256 Sherbrooke, and (iv) soil datasets from the Research and Development Institute for the Agri-
 257 environment. Daily meteorological data, including precipitation, minimum and maximum
 258 temperature covering the 1963-2020 period, were extracted from Environment and Climate
 259 Change Canada's database using the package *weathercan* in R (v.4.0.4). A radius of 75 km (St.
 260 Charles) and 100 km (Bécancour) from the center of each watershed was used to select the
 261 meteorological stations. A total of 28 stations were considered for the St. Charles watershed, while
 262 63 stations were included for the Bécancour watershed. For the St. Charles, precipitation data
 263 from 31 rain gauges operated by Quebec City were also included in the meteorological dataset.

264 To prepare the physiographic database, PHYSITEL: (i) calculates the slope and flow direction for
 265 each cell, (ii) processes the flow accumulation matrix, (iii) discretizes the watershed into hillslopes,
 266 (iv) for each hillslope, determines the percentage of each land cover and the dominant soil texture.
 267 Accounting for wetlands in HYDROTEL also requires PHYSITEL to: (i) identify wetlands from the
 268 land cover map, (ii) calculate the maximum area of wetlands from the number of pixels associated
 269 to the wetland class, (iii) delineate the CA of each wetland using the accumulation matrix, (iv)
 270 differentiate IWs and RWs based on a river network adjacency threshold, and for each hillslope
 271 (v) merge wetlands into one isolated and/or one riparian hydrologically equivalent wetland (HEW;
 272 Wang et al., 2008). During the latter step, PHYSITEL provides the total area of all the wetlands
 273 belonging to a specific typology (IW or RW) to calculate the wetland maximum surface area
 274 ($SA_{wet,max}$) and also the total CA of each HEW to assess the fraction of the hillslope that is

275 contributing to the HEW (fr_{wet}). In addition, PHYSITEL spatially connects the riparian HEWs at
276 specific locations on the river reaches.

277 For the HEW of the IW and RW computational modules, HYDROTEL computes the water budget
278 using Equations (1) and (2), respectively:

$$279 \quad V_{wet2} = V_{wet1} + V_{pcp} - V_{ev} - V_{seep} - V_{fout} + V_{fin} \quad (1)$$

$$280 \quad V_{wet2} = V_{wet1} + V_{pcp} - V_{ev} - V_{seep} - V_{ex} + V_{fin} \quad (2)$$

281 where V_{wet2} and V_{wet1} are volumes of water stored at the end and beginning of a time step (m^3 ;
282 $V_{wet1} = V_{wet,nor}$ at the first time step, see Equation (8)), V_{pcp} is the volume of precipitation received
283 (m^3), V_{ev} is the volume of water lost to evapotranspiration, estimated as a percentage of the
284 evapotranspiration at hillslope scale, V_{seep} is the water transferred to a deep aquifer calculated
285 using Darcy's law and transferred to the terrestrial flow (IW) or the river water routing (RW)
286 modules to close the hydrological budget, V_{fout} is the volume of water leaving the isolated HEW
287 and is calculated using an iterative scheme (see Fossey et al. (2015) for additional details), and
288 V_{ex} is the volume of water exchanged between the riparian HEW and the river reach (calculated
289 by iteration, using Darcy's law and assuming that the HEW and river water levels are equal at the
290 end of the time step). Finally, V_{fin} (Equation (3)) is the water entering the HEW from the vertical
291 water budget:

$$292 \quad V_{fin} = Q_{hillslope} \times (fr_{wet} \times SA_{hillslope} - SA_{wet}) \times 10 \quad (3)$$

293 where $Q_{hillslope}$ is the sum of surface, lateral, and base flows (mm) calculated in the vertical water
294 budget, fr_{wet} is the percentage of wetland CA for each hillslope, $SA_{hillslope}$ is the area of each
295 hillslope (m^2), and 10 is a conversion factor ($SA_{hillslope}$ and SA_{wet} are first converted to ha;
296 $m^3/(ha.mm)$). SA_{wet} is the area of wetland updated at every computational time-step, using
297 Equation (4):

$$298 \quad SA_{wet} = \beta \times V_{wet}^{\alpha} \quad (4)$$

299 where α and β are:

$$300 \quad \alpha = \frac{\log_{10}(SA_{wet,max}) - \log_{10}(SA_{wet,nor})}{\log_{10}(V_{wet,max}) - \log_{10}(V_{wet,nor})} \quad (5)$$

$$301 \quad \beta = \frac{SA_{wet,max}}{V_{wet,max}^{\alpha}} \quad (6)$$

302 In Equations (5) and (6), $SA_{wet,max}$ is the area of a HEW (calculated in PHYSITEL) when the water
303 is at maximum level ($WETDMAX$) and $SA_{wet,nor}$ is the area when the water is at normal level ($WETDNOR$),
304 which corresponds to a percentage ($FRAC$) of $SA_{wet,max}$. $V_{wet,max}$ and $V_{wet,nor}$ are
305 calculated using Equations (7) and (8), respectively:

$$306 \quad V_{wet,max} = WETDMAX \times SA_{wet,max} \quad (7)$$

$$307 \quad V_{wet,nor} = WETDNOR \times SA_{wet,nor} \quad (8)$$

308 **2.3. Model calibration**

309 The parameters of the HYDROTEL modules (Supplemental material, Table S1) were
 310 automatically calibrated (budget of 250 iterations, 10 trials) using the Asynchronous Parallel multi-
 311 objective optimization algorithm Pareto Archived Dynamically Dimensioned Search (ParaPADDs;
 312 Asadzaded and Tolson, 2009; Tolson et al., 2014) provided with the Optimization Software Toolkit
 313 for Research Involving Computational Heuristics (OSTRICH v17.12.19
 314 <http://www.civil.uwaterloo.ca/envmodelling/Ostrich.html>; Matott, 2017). To minimize initialization
 315 errors and account for the water balance warm-up, the first year was removed prior to the
 316 calculation of the objective functions. In addition, winter stream flows (November to March; ice-on
 317 period) were excluded from the calibration since the uncertainty related to measurements during
 318 this period is high. Daily observed stream flows provided by the CEHQ (Fig. 1) were compared
 319 with daily simulated stream flows using the KGE (Gupta et al., 2009) and NSE-LOG (Oudin et al.,
 320 2006) as objective functions, calculated with the R package *hydroGOF* (R Core Team, 2020;
 321 Zambrano-Bigiarini, 2020) and the Python package *hydroeval* (Hallouin, 2021). For the St. Charles
 322 watershed, a sub-watershed calibration strategy was implemented, meaning that each sub-
 323 watershed (except the St. Charles sub-watershed) was calibrated independently. The values of
 324 the parameters of the Nelson, Des Hurons and Jaune River being set, the final calibration involved
 325 the area between the outlets of the subwatersheds and that of the St. Charles sub-watershed
 326 using the daily observed stream flows of station 090504 (Fig. 1). For this specific station, a water
 327 intake was considered in the calibration process and an ecological stream flow (0.33 m³/s) needed
 328 to be met for the whole period of calibration. The Bécancour watershed was calibrated between
 329 January 1st 2004 and December 31st 2015, using daily observed stream flows at station 024014
 330 (Fig. 1; Ministère de l'Environnement et la Lutte contre les Changements Climatiques, 2021). For
 331 this watershed, data on water withdrawals (which come from underground sources) or ecological
 332 stream flow were unavailable, so they were not accounted for by HYDROTEL. The calibration
 333 exercise was deemed satisfactory and characterized by good performance metrics for the different
 334 river reaches under study (Table 1).

335 **Table 1. Hydrometric station used for calibration purpose, period of data availability, and calibration**
 336 **performance metrics for each watershed/sub-watershed. KGE: Kling and Gupta**
 337 **Efficiency criteria (Gupta et al., 2009). NSE-LOG: Nash-Sutcliffe efficiency criterion**
 338 **calculated on log-transformed flows (Oudin et al., 2006). PBIAS: percent-bias (Yapo**
 339 **et al., 1996). RMSE: Root-mean square error (Singh et al., 2005).**

Watershed/Sub-watershed	Period	KGE	NSE-LOG	PBIAS (%)	RMSE (m ³ /s)
Des Hurons (050916)	2007-2020	0.74	0.76	-14.38	2.69
Jaune (050906)	1983-1994	0.78	0.69	-13.93	1.84
Nelson (050915)	2006-2020	0.79	0.77	-14.03	1.08
Lorette (050914)	2006-2009	0.83	0.79	-4.53	1.57

Du Berger (050907)	1983-1995	0.72	0.49	-21.67	1.14
St. Charles (050904)	2000-2020	0.75	0.73	-20.18	7.30
Becancour (024014)	2004-2015	0.91	0.87	-1.11	30.19

340

341 **2.4. Sensitivity analysis**342 **2.4.1. VARS toolbox theoretical background**

343 Parameter sensitivity was assessed using the Variogram Analysis of Response Surface (VARS)
 344 toolbox (Razavi et al., 2019), which is compatible with any model through a connection with
 345 OSTRICH (Matott, 2017). Inspired by the variogram techniques that are of common usage in
 346 geostatistical analyses, VARS is a recently developed GSA method where the response surface
 347 of the model is considered as a spatially distributed dependent variable. It recognizes that there
 348 is a spatial and continuous covariance structure in the model response. A variogram (γ ; Equation
 349 (9)) describes this spatial covariance structure for a given stochastic process:

$$350 \quad \gamma(h) = \frac{1}{2|N(h)|} \sum_{(i,j) \in N(h)} (y(x^A) - y(x^B))^2 \quad (9)$$

351 where h is the variogram scale (distance between computational points), $N(h)$ is the number of
 352 pairs of points that are h -distant, $y(x^A)$ and $y(x^B)$ are the model responses in the parametric space
 353 at location x^A and x^B , respectively. In the context of a GSA, the VARS method consists of
 354 generating a variogram for each parameter. Thus, higher $\gamma(h_i)$ values indicate a higher sensitivity
 355 in the direction of parameter i (Razavi and Gupta, 2016a). The sensitivity index associated with
 356 the VARS method is the integrated variogram (IVAR; Equation (10)):

$$357 \quad \Gamma(H_i) = \int_0^{H_i} \gamma(h_i) dh_i \quad (10)$$

358 for a scale interval from 0 to H_i and for parameter i . As suggested by the authors, values
 359 associated with a 50% interval (IVAR50) were used in this study. The relative sensitivity (IVAR50n)
 360 presented throughout the paper is calculated as follows:

$$361 \quad IVAR50n = \frac{IVAR50_i}{\sum_i^n IVAR50_i} \quad (11)$$

362 **2.4.2. Sensitivity analyses of the wetland modules**

363 The SA focused on the parameters of the wetland modules. As a first step, the “star-based”
 364 sampling strategy included in the VARS toolbox was used to generate the parameter sets,
 365 according to the lower and upper bounds reported in Table 2. This framework generates
 366 parameter sets covering all the parametric space and facilitates the computation of sensitivity
 367 metrics (Razavi and Gupta, 2016b). The strategy consists of: (i) randomly generating m points
 368 (star centers) across the factor space, and (ii) aligning equally spaced points along each

369 dimension (i.e., parameters, n) in the factor space (based on a user defined sampling resolution;
370 Δh). Following these steps, the final number of parameter sets (r) is:

$$371 \quad r = m \left(n \left(\frac{1}{\Delta h} - 1 \right) + 1 \right) \quad (12)$$

372 In this study, we used 50 stars, a sampling resolution of 0.1, and the latin hypercube sampling to
373 generate the parameter sets. Second, for each parameter set we ran the model using the Model
374 Evaluation program integrated in the parallelized version of OSTRICH using supercomputers
375 Beluga and Narval, managed by Calcul Québec and the Digital Research Alliance of Canada. The
376 model was run from January 1st, 1999, to December 31st, 2020, and a 365-day spin-up period was
377 removed from the beginning of the resulting time series to minimize initialization errors. Third, to
378 account for sensitivity temporal variability, we calculated daily mean sensitivity indices over the
379 2000-2020 period (i.e., IVAR50) using VARS and the Generalized Global Sensitivity Matrix
380 (GGSM) in MATLAB (R2018b).

381 To assess wetland parameter sensitivity at the hillslope scale as well as the watershed scale, we
382 then performed two categories of SAs (Fig. 4). First, to assess how a variation in the value of
383 parameters affects the outflow of the wetland modules ($V_{f_{out}}$ and V_{ex}), that is the hillslope/HEW
384 scale, a SA was conducted for specific HEWs located in the Jaune River sub-watershed. Based
385 on the definition of wetland networks suggested by Blanchette et al. (2022) which is described in
386 terms of specific wetland area and CA criteria, four isolated HEWs and four riparian HEWs were
387 selected (Fig. 5). For each typology (i.e., isolated and riparian), the four wetlands belonged to one
388 of the following networks: small wetland with small CA into the small wetlands group (PI), small
389 wetland with large CA into the small wetlands group (PII), large wetland with small CA into the
390 large wetlands group (PIII), and large wetland with large CA into the large wetlands group (PIV).
391 The selected wetlands were hydrologically independent from each other. Then, HYDROTEL was
392 run using 2750 and 2300 parameter sets and IVAR50 was computed on $V_{f_{out}}$ and V_{ex} , for IWs
393 and RWs, respectively. Second, SAs were performed at both the watershed scale and the sub-
394 watershed scale, using 5000 parameter sets. The parameters of both wetland modules were
395 varied simultaneously for this analysis. For the St. Charles River watershed, IVAR50 was
396 calculated using the simulated outlet flows of the watershed and each sub-watershed. Moreover,
397 in line with the calibration strategy, for the simulated stream flows at the outlet of the watershed,
398 a water withdrawal (data provided by Quebec City) was removed from simulated data and a
399 minimum ecological flow of 0.33 m³/s was enforced. For the Bécancour River watershed, IVAR50n
400 was calculated on simulated stream flows at station 024014. To account for the impact of wetland
401 location on the variability of wetland parameter sensitivities, we divided the wetlands of each study
402 watershed by Strahler order. The Strahler order classification (Strahler, 1957) is used to quantify
403 the structure of a hydrographic network and the relative location of each river reach. It can be used
404 as an indicator of stream size (Hughes et al., 2011). The reaches head are assigned a value of 1
405 which goes up at each branch. We identified the Strahler order of each river reach and assigned
406 it to the corresponding hillslopes, using ArcMAP (v10.6.1, www.esri.com; Environmental Systems
407 Research Institute (ESRI), 2018). We used the list of hillslopes to assign a Strahler order to each
408 isolated HEW and each riparian HEW. We then created HYDROTEL projects containing only the
409 wetlands corresponding to specific Strahler orders by modifying the files describing wetlands
410 (comma-separated files listing wetland parameters and HEW spatial characteristics for each
411 hillslope or river reach, for IWs and RWs respectively). For example, in the case of wetlands
412 associated with 1st order river reaches, only them were included in the simulation, that is wetlands
413 of Strahler order 2 or higher were not simulated in the model. This resulted in five SA projects for
414 the Bécancour River watershed (all wetlands, Strahler order 1 to 4) and six projects for the St.

415 Charles River watershed (all wetlands, Strahler order 1 to 5). All those projects were evaluated
416 with the same list of 5000 parameter sets using the supercomputers.

417 **Table 2. Description of the wetland parameters in HYDROTEL, and lower and upper bounds used for**
418 **the sensitivity analyses.**

Parameters	Category	Bounds	Description
<i>FRAC-IW</i>	Geometry	[0.20 ; 0.60]	Ratio defining the relationship between the HEW surfaces at the wetland maximum and normal water levels, respectively (%)
<i>KSATBS-IW</i>	Hydrogeology	[0.25 ; 0.75]	Saturated hydraulic conductivity of the soil beneath the HEW (mm/h)
<i>WETDNOR-IW</i>	Geometry	[0.05 ; 0.25]	Threshold values of water depth in the HEW corresponding to the normal level (m)
<i>WETDMAX-IW</i>	Geometry	[0.25 ; 1.30]	Threshold values of water depth in the HEW corresponding to the maximum level (m)
<i>CEV-IW</i>	Hydrology	[0.30 ; 0.90]	Evaporation from HEW defined as a percentage of potential evapotranspiration calculated at RHHU scale (%)
<i>CPROD-IW</i>	Hydrology	[5.00 ; 15.00]	Contribution of HEW to terrestrial flow defined as a percentage of wetland water volume when the water level is between the normal and maximum levels (%)
<i>FRAC-RW</i>	Geometry	[0.20 ; 0.60]	Ratio defining the relationship between HEW surfaces at the wetland maximum and normal water levels, respectively (%)
<i>KSATBS-RW</i>	Hydrogeology	[0.25 ; 0.75]	Saturated hydraulic conductivity of the soil beneath the HEW (mm/h)
<i>WETDNOR-RW</i>	Geometry	[0.05 ; 0.25]	Threshold values of water depth in the HEW corresponding to the normal level (m)
<i>WETDMAX-RW</i>	Geometry	[0.25 ; 1.30]	Threshold values of water depth in the HEW corresponding to the maximum level (m)
<i>KSATBK-RW</i>	Hydrogeology	[12.50 ; 37.50]	Bank saturated hydraulic conductivity (mm/h)

419

420

421 **Fig. 4. Methodological flow chart of the two categories of sensitivity analysis.**

422 **Fig. 5. Location of the HEWs selected to assess parameter sensitivity at hillslope/HEW scale.**

423 **3. Results**

424 **3.1. Parameter sensitivity at the hillslope/HEW scale**

425 The parameter sensitivity at the hillslope/HEW scale varies for IWs and RWs. For both wetland
 426 modules (Fig. 6), the geometry parameters, defined by *FRAC-IW*, *FRAC-RW*, *WETDNOR-IW*,
 427 *WETDNOR-RW*, *WETDMAX-IW*, and *WETDMAX-RW* largely explains the parametric sensitivity
 428 of wetland outflow. For IWs and RWs, they explain 59-67% and 83-97% of the sensitivity,
 429 respectively. Indeed, the geometry of wetlands directly affects the volume of water they can store
 430 and modulates hillslope hydrology (local scale) and watershed hydrology (Jones et al., 2018;
 431 McLaughlin et al., 2014). For IWs, *CEV-IW* and *CPROD-IW* explain 6-25% of the sensitivity, which
 432 indicates the low sensitivity of the geometric parameters for this specific typology. Soil parameters
 433 (*KSATBS-IW*, *KSATBS-RW*, and *KSATBK-IW*) account for 15-28% of the sensitivity for IWs and
 434 2-17% for RWs.

435 The contribution of each parameter to the global sensitivity at the outlet of the HEWs is variable
 436 across the wetland spatial configurations, and even intra-typologies (i.e., IW or RW). For IWs,
 437 *WETDMAX-IW* has a much higher sensitivity for wetlands with larger CAs (IVAR50n = 0.57 and
 438 0.53, for PII and PIV respectively), suggesting that the outflow from IWs hydrologically fed by a
 439 large area is closely related to their maximum water depth. Moreover, IWs with larger CAs are
 440 more sensitive to *CPROD-IW* (contribution of HEW to terrestrial flow). Conversely, for IWs with
 441 smaller CAs, the outflow is more sensitive to *FRAC-IW* (IVAR50n = 0.32 and 0.29, for PI and PIII,
 442 respectively) and *WETDNOR-IW* (IVAR50n = 0.23 and 0.21, for PI and PIII, respectively), two
 443 parameters related to normal flow conditions. IWs with smaller CAs highly rely on precipitation
 444 input to store water, as they cannot rely on runoff from their CAs. Consequently, their surface area
 445 strongly affects their capacity to store water and the volume of outflows. For RWs, *WETDNOR-*
 446 *RW* is more sensitive for small wetlands with small CAs (PI) and large wetlands with large CAs
 447 (PIV), while wetlands with average spatial characteristics (PII and PIII) are more sensitive to
 448 *WETDMAX-RW*. Additionally, only large wetlands with large CAs are sensitive to *KSATBK-RW*.
 449 These results highlight the impact of the spatial configuration (area/CA) of a wetland on its
 450 hydrological behavior at the hillslope scale.

451 **Fig. 6. Relative sensitivity index (IVAR50n) for the wetland scale sensitivity analysis project. PI: small**
 452 **wetland, small contributing area (CA). PII: small wetland, large CA, PIII: large wetland,**
 453 **small CA, PIV: large wetland, large CA.**

454 **3.2. Parameter sensitivity at the watershed scale**

455 At the outlet of the St. Charles watershed (6% wetland cover), considering all typologies of
 456 wetlands and all Strahler orders, the most sensitive parameters are *FRAC-RW*, *WETDNOR-RW*
 457 and *KSATBS-RW*, which all belong to the RW module (Table 3). These dominant parameters are
 458 in line with the surface area of RWs (3.2%), which is 1.4 times more abundant than that of IWs
 459 (2.5%) at watershed scale (CAs are 13% for both). The least sensitive parameters are *FRAC-IW*,
 460 *CEV-IW* and *WETDNOR-IW*.

461 On the other hand, the proportion of land cover by isolated and riparian HEWs also clearly drives
 462 the Bécancour sensitivity rankings. At the hydrometric station of the Bécancour River, the most
 463 sensitive parameters all belong to the IW module (*WETDNOR-IW*, *KSATBS-IW* and *CPROD-IW*)

464 while the five least sensitive parameters are those of the RW module. This reflects a clear
 465 correlation with the dominant typology of wetlands at watershed scale, where IWs (7.5% draining
 466 28% of the watershed) are 3.75 times more abundant than RWs (2% draining 7% of the
 467 watershed). For both watersheds, *KSATBK-RW* is the least sensitive parameter. The contribution
 468 of this parameter is limited to a specific case of the iterative scheme (Fossey et al., 2015); it
 469 weakens its sensitivity compared to the other parameters.

470 **Table 3. Rank of IVAR50n sensitivity index on the parameters of the wetland modules of HYDROTEL**
 471 **for the simulated stream flows at the outlet of the St. Charles River watershed, and**
 472 **at station 024014 of the Bécancour River.**

Parameters	St.Charles	Bécancour
FRAC-IW	9	4
KSATBS-IW	7	2
WETDNOR-IW	8	1
WETDMAX-IW	4	5
FRAC-RW	1	8
KSATBS-RW	3	9
WETDNOR-RW	2	7
WETDMAX-RW	5	10
CEV-IW	10	6
CPROD-IW	6	3
KSATBK-RW	11	11

473

474

475 **3.2.1. Spatial variability of parameter sensitivity at watershed and sub-watershed**
 476 **scales**

477
 478 **Fig. 7 IVAR50n wetland module sensitivity indices for the simulated stream flows of wetlandscapes**
 479 **defined by Strahler order at (a) the outlet of the St. Charles River watershed, and (b)**
 480 **at station 024014 of the Bécancour River.**

481 At the outlet of the St. Charles River (Fig. 7 (a)), when considering the wetlands associated with
 482 river reaches of Strahler order I, *WETDMAX-IW* and *CPROD-IW* present the highest sensitivities
 483 with IVAR50n values reaching 0.23 and 0.17, respectively. These two parameters become
 484 impactful during high precipitation events and/or snowmelt season. Additionally, the high
 485 sensitivities of those parameters for IWs related to headwater streams suggests their wetlands
 486 might have a strong impact on mitigating downstream peak flows. For wetlands of Strahler orders
 487 II, III and V, the RW parameters display a substantially high sensitivity, with *FRAC-RW* being the
 488 most sensitive parameter with IVAR50n values of 0.25, 0.28 and 0.25, respectively. As mentioned
 489 previously, *FRAC* is a very important parameter for both wetland modules, as it connects $SA_{wet,max}$
 490 to $SA_{wet,nor}$, two variables that interact in the calculation of SA_{wet} at every time-step and ultimately
 491 to the volume of stored water. For Strahler order II, *WETDNOR-RW* is also among the most
 492 sensitive parameters, followed by *WETDMAX-RW*, which highlights the importance of the
 493 geometric parameters once more. Considering Strahler order III wetlands, the most sensitive
 494 parameters are *FRAC-RW* (0.28), *KSATBS-RW* (0.21) and *WETDNOR-RW* (0.20). First, these
 495 results reveal that while increasing stream order, RW parameters become more sensitive
 496 compared to the IW parameters. Second, they also depict that for RWs located on stream order
 497 III, river flows are less influenced by changes in their maximum capacity to store water (defined
 498 by *WETDMAX-RW*) but seem rather driven by parameters associated with average (*WETDNOR-*
 499 *RW*) or low (*KSATBS-RW*) flow conditions, compared to RW located on Strahler order II. For
 500 Strahler order IV, the most sensitive parameters are shared between the two wetland typologies:
 501 *KSATBS-IW* (0.15), *WETDMAX-RW* (0.14), and *FRAC-IW* (0.13) and *WETDNOR-IW* (0.13) are
 502 ranked in the top three. The dominant typology for each Strahler order seems to drive the spectrum
 503 of sensitivity among parameters of the two modules. Indeed, RWs are dominant for Strahler orders
 504 II, III and V (see total wetland area; Fig. 2), while the ratio of IW to RW areas for Strahler order I
 505 and IV is close to 1:1. However, the ratio of CA is highly dominated by IWs, which could explain
 506 the high sensitivity of IW parameters for these Strahler orders.

507 For the Bécancour River watershed (Fig. 7 (b)), parameters related to the IW module are more
 508 sensitive among all Strahler orders than those of the RW module. This is expected, considering
 509 the higher land cover of IWs on this watershed, which is always at least twice that of RWs. For the
 510 Strahler orders II and III with nearly a 2:1 ratio, IVAR50n indices for RWs are slightly higher than
 511 those for Strahler orders I and IV. Conversely, for Strahler IV wetlands, there is only 0.03% of
 512 RWs for 1.85% of IWs. That is reflected in the values of IVAR50n, reaching the maximum value
 513 (0.29) among all HYDROTEL projects at watershed scale for *WETDNOR-IW* and *KSATBS-IW*.
 514 Finally, considering all Strahler order projects and for both watersheds, the time-aggregated value
 515 of *KSATBK-RW* relative sensitivity is consistently lower than 0.01.

516 The effect of wetland typology on sensitivity rankings is even more convincing at the sub-
 517 watershed scale. For sub-watersheds where there is a clear dominant typology, the parameters
 518 related to this type of wetlands consistently have higher sensitivities when compared to those of
 519 the non-dominant typology. When ordering the results for each sub-watershed/Strahler order
 520 project in ascending order of the ratios between IW and RW areas (Fig. 8), this behavioral

521 relationship becomes even more obvious. This representation also highlights a threshold
 522 corresponding to a 1:1 ratio, above which IWs become dominant, as do their parameters. The
 523 results also suggest that, although *KSATBS-RW* was not highly sensitive at wetland scale (section
 524 3.1), its relative sensitivity metric increases considerably when investigating its impact at the
 525 watershed and sub-watershed scales. These results highlight the impact of location (wetland vs
 526 watershed scale, upstream vs downstream gradient) and especially typology on parameter
 527 sensitivity.

528 **Fig. 8 IVAR50n wetland module sensitivity indices for simulated stream flows of wetlandscapes**
 529 **defined by Strahler order at the outlet of the St. Charles River sub-watersheds: HUR:**
 530 **des Hurons, NEL: Nelson, JAU: Jaune, DUB: du Berger, LOR: Lorette. I, II, III and IV**
 531 **refer to the Strahler order.**

532 3.2.2. Temporal variability of parameter sensitivity at watershed scale

533 At watershed (and sub-watershed) scales, the sensitivity of stream flows to wetland parameters
 534 reveals a strong temporal variability, which follows the seasonality of the different hydrological
 535 processes occurring in HEWs. For the St. Charles watershed (Fig. 9), while *FRAC-IW*, *FRAC-RW*,
 536 *KSATBS-IW*, *KSATBS-RW*, *WETDNOR-IW*, and *WETDNOR-RW* exhibit high frequency
 537 variations (daily), they also present a substantial decrease in mean sensitivity (calculated over the
 538 2000-2020 period) during the spring snowmelt season (\approx DOY 120), where *WETDMAX-IW* and
 539 *WETDMAX-RW* peak. Although *WETDMAX-IW* and *WETDMAX-RW* are not in the top three
 540 parameters when considering the watershed scale time-aggregated sensitivity index (*WETDMAX*
 541 is ranked 4th and 5th for IW and RW, respectively, Table 3), the daily mean IVAR50n shows the
 542 strong influence of this parameter during spring. In temperate regions, during spring, snowmelt is
 543 the dominant hydrological process. During this time of the year, wetland storage is generally at
 544 capacity and any exceeding inflow leads to wetland overflow that will reach the river network and
 545 affect stream flows. Therefore, the maximum water table depth is highly sensitive under these
 546 conditions because it directly affects the capacity of the HEW to store water. This not only confirms
 547 the relevance of investigating temporal sensitivity (Gupta and Razavi, 2018; Razavi and Gupta,
 548 2019), but it also implies that, at the peak of the spring snowmelt, the variability in stream flows at
 549 the outlet of this watershed highly depends on the capacity of wetlands to store water.
 550 Consequently, increasing or reducing this capacity (hereby characterized by its maximum depth)
 551 will influence output flows. The peak sensitivity for *WETDMAX-IW* is delayed (\approx day of the year,
 552 DOY, 150) compared with the peak sensitivity for *WETDMAX-RW* which occurs around DOY 125.
 553 This suggests that IWs may retain water longer than RWs, the latter being directly connected to
 554 the hydrographic network. Therefore, when the water level in a RW reaches a certain threshold,
 555 water transfers to the river. The proximity and connection between RWs and the river imply a high
 556 reactivity during the spring snowmelt season. However, this delayed peak in sensitivity does not
 557 appear for the Bécancour River (Fig. 10). For this watershed, most of the sensitivity relies on the
 558 parameters of the IWs, which account for 79% of wetland area at watershed scale. Accordingly,
 559 *WETDMAX-IW* sensitivity peak is much higher than that of *WETDMAX-RW*. Considering
 560 hydrogeological parameters (*KSATBS-IW*, *KSATBS-RW* and *KSATBK-RW*), results show that
 561 IVAR50n remains stable for *KSATBS-IW* and *KSATBS-RW* for the St. Charles watershed during
 562 most of the year, except during the spring snowmelt, where, as mentioned previously, *WETDMAX-*
 563 *RW* becomes the dominant parameter. For the Bécancour watershed, IVAR50n ranges from 0.00
 564 to 0.50 for *KSATBS-IW*, with slightly higher values during winter, and values lower than 0.10 for
 565 *KSATBS-RW*. For both watersheds, *KSATBK-RW* is null throughout the year, which confirms that
 566 this parameter could be set in the RWs module. Finally, looking more precisely at parameters
 567 related to the hydrological budget, the relative sensitivity of *CPROD-IW* increases during spring
 568 and fall. The relative sensitivity ranges between 0 and 0.30 for *CEV-IW* in both watersheds, with

569 almost null sensitivity beyond summer. In Canada, 65% of the annual evapotranspiration occurs
 570 over three months, that is June, July, and August, and in the Boreal Shield ecozone,
 571 evapotranspiration peaks in July (Wang et al., 2013). Thus, during summer, substantial loss of
 572 water through evapotranspiration affects stream flows. While CEV-IW represents the percentage
 573 of evapotranspiration at the RHHU scale, varying the value of this parameter directly affects the
 574 volume of water lost to the atmosphere at the HEW scale (V_{ev}), which in return, has an impact on
 575 stream flows at the watershed scale.

576 Comparing the relative sensitivities between the St. Charles and the Bécancour watersheds, it
 577 becomes evident that the stream flows at the outlet of the St. Charles River has a higher sensitivity
 578 to parameters characterizing high hydrological conditions (*WETDMAX-IW* and *WETDMAX-RW*),
 579 while stream flows on the Bécancour seem more sensitive to parameters related to normal (*FRAC-*
 580 *IW*, *FRAC-RW*, *WETDNOR-IW*, and *WETDNOR-RW*) and low (*KSATBS-IW*) hydrological
 581 conditions. Aside from their different surface area ratios of IWs versus RWs, this outcome might
 582 be explained by an insufficient wetland cover in the St. Charles River watershed to maintain so-
 583 called normal wetland hydrological conditions. Wetlands of this watershed may therefore fill and
 584 overflow faster than those of the Bécancour River. Consequently, wetlands of the St. Charles
 585 watershed are more sensitive to *WETDMAX*. Repeating a similar methodology on watersheds
 586 characterized by a variety of wetland covers could help refine these assumptions.

587 **Fig. 9. Daily IVAR50n mean values (black line) and interval between 10th and 90th quantiles (grey**
 588 **areas), calculated over the 2000-2020 period, considering all wetlands, on stream**
 589 **flows at the outlet of the St. Charles River watershed for: (a) the isolated wetlands**
 590 **parameters, and (b) the riparian wetlands parameters. The vertical bold, white, dotted**
 591 **lines mark the beginning of hydrometeorological seasons: March 1st (spring), June**
 592 **1st (summer), September 1st (fall), and December 1st (winter). DOY: day of year.**

593 **Fig. 10. Daily IVAR50n mean values (black line) and interval between 10th and 90th quantiles (grey**
 594 **areas), calculated over the 2000-2020 period, considering all wetlands, on stream**
 595 **flows at the station 024014 of the Bécancour River for: (a) the isolated wetlands**
 596 **parameters, and (b) the riparian wetlands parameters. The vertical bold white dotted**
 597 **lines mark the beginning of hydrometeorological seasons: March 1st (spring), June**
 598 **1st (summer), September 1st (fall), and December 1st (winter). DOY: day of year.**

599 Observing the sensitivity temporal variability for *WETDMAX-IW* specifically along a Strahler order
 600 (STR) gradient, we can see that IVAR50n peak occurs during spring, decreases from STR1 to
 601 STR4, and disappears completely with STR5 (Fig. 11 (a)). *WETDMAX-RW* shows the opposite
 602 behavior (Fig. 11 (b)): peak sensitivity increases from STR1 to STR3 and stabilizes for STR4 and
 603 STR5. These results corroborate those of Fossey et al. (2016) regarding wetlands of the
 604 Bécancour River watershed, where upstream IWs had a greater effect on modulating stream
 605 flows, while downstream RWs connected to the main stream were more efficient.

606 **Fig. 11. Daily IVAR50n mean value for the parameters *WETDMAX-IW* (left) and *WETDMAX-RW* (right)**
 607 **for each Strahler order related wetlands, at the outlet of the St. Charles River**
 608 **watershed (black line), and at station 024014 of the Bécancour River (grey line). See**
 609 **Fig. S1 for the outlet of the St. Charles River sub-watersheds. DOY: day of year.**

610 4. Discussion

611 Understanding how parameters interact in a model and affect outputs is essential to support the
 612 interpretation of simulation results. Not only can it help refine model parameterization, but it also
 613 provides key insights on the modelled system. In this paper, we presented the results of a GSA
 614 performed on the wetland modules of the hydrological modelling platform PHYSITEL/HYDROTEL.

615 Using two case-study watersheds along with the recently developed VARS toolbox, we
616 implemented a spatio-temporal GSA to quantitatively assess how wetland parameters affect
617 simulation outputs and to guide future data acquisition field campaign to improve the
618 representation of wetland-related processes in the model.

619 Our study demonstrated the dominant impact of geometric parameters at both the wetland scale
620 (i.e., hillslope/HEW scale) and the watershed scale. These parameters, which include *FRAC*,
621 *WETDMAX* and *WETDNOR*, participate in the calculation of the wetland water storage and
622 wetland surface area at every computational time-step. Such findings corroborate those of
623 McLaughlin et al. (2014), among others (Fossey et al., 2015; Liu et al., 2008), who highlighted the
624 importance of wetland geometry on stream flows. However, our results suggest that the relative
625 sensitivity among these parameters varies with wetland configurations (i.e., wetland extent and
626 CA), when investigating parameter sensitivity at the wetland scale. In terms of wetland
627 management, this raises important questions, as wetlands with different spatial configurations
628 could respond differently to similar changes in their areas (*FRAC*) or depth (*WETDNOR* and
629 *WETDMAX*). Although we previously performed a quantitative assessment of how wetland area
630 and CA affect stream flows (Blanchette et al., 2022), performing an exhaustive GSA on scenarios
631 of various wetland spatial configurations could prove to be useful to transfer our conclusions at
632 watershed scale.

633 The methodological framework presented in this study also demonstrated that the ratio of surface
634 area of IW to RW strongly affects the ranking of sensitivity among wetland parameters at the
635 watershed scale. Accordingly, in watersheds dominated by IWs, the sensitivity of stream flows will
636 be mostly attributed to IW parameters, while watersheds where the extent of RWs exceed IW area
637 they will exhibit higher sensitivity for RW parameters. This finding nuances results found in the
638 literature giving more impact to upstream IW compared to RW for mitigating high flows (Fossey et
639 al., 2016), and underlines the importance of wetland hydroconnectivity. Our results also indicate
640 that wetland hydroconnectivity appears to impact stream flow sensitivity differently along a
641 continuum of Strahler orders, especially when considering geometric parameters (e.g.,
642 *WETDMAX*). Indeed, IWs display higher sensitivities upstream (low Strahler order) than
643 downstream (high Strahler order), while RWs display the opposite behavior. Notwithstanding
644 these findings were expected, notably considering recent studies performed using HYDROTEL
645 (Fossey et al., 2015; Fossey et al., 2016), they are highly relevant in the context where setting
646 wetland conservation and restoration targets at watershed scale remains a challenge. For
647 instance, protecting IWs located upstream constitutes an efficient mean of attenuating high flows
648 and supporting low flows. Keeping in mind that changing geometrical characteristics of wetlands
649 influences wetland outflows and river flows, any wetland management strategy affecting the
650 geometry of a wetland (depth, area, subsurface geometry) will impact stream flows more strongly
651 if upstream IWs are targeted, while changes in IW geometry downstream will have a lesser impact.

652 All the above findings are particularly relevant in the context where model improvements rely on
653 field data acquisition. Knowing that geometric parameters are the most sensitive, data acquisition
654 campaign should focus on water level monitoring, subsurface delineation, and extent mapping
655 under various conditions. Considering that IWs located upstream are more sensitive to their
656 geometric characteristics than downstream IWs, HYDROTEL could benefit from field data
657 monitoring targeting IWs located on headwater RHHUs. Conversely, the geometric parameters of
658 the RW module revealed a higher sensitivity for wetlands adjacent to the main channel (\geq STR3).
659 Thus, water level monitoring should focus on downstream sites. Additionally, the high relative
660 sensitivity of *WETDMAX* during the spring snowmelt points towards monitoring water levels at that
661 time of the year especially. Inversely, saturated hydraulic conductivity measurements (*KSATBS*)
662 should take place under low hydrological conditions (e.g., summer or winter) since this parameter

663 shows higher sensitivity metrics during these seasons. Other parameters, such as *FRAC* remain
664 highly sensitive throughout the year since they are involved in the computation of wetland area at
665 every time-step. This confirms the relevance of having access to high-resolution wetland maps.
666 Nowadays, the refinement of remotely sensed technologies has enabled the development of earth
667 imaging with increased precisions. For example, Xi et al. (2022) released an ensemble of 28
668 gridded maps of monthly global/regional wetland extents for 1980-2020 with a spatial resolution
669 of 0.25°. In combination with water-level time series, these maps could improve the quantification
670 of *FRAC*, *WETDMAX* and *WETDNOR* in various landscapes.

671 The spatial variability of wetland parameter sensitivity emphasizes the need to reproduce this
672 exercise for any new model implementation. Nevertheless, the extraction of general rules based
673 on the dominant typology and location in the watershed to refine wetland parameter calibration
674 deserves to be explored. Replicating this method under different geological conditions could help
675 refine our understanding of the spatio-temporal variability of the wetland parameters sensitivity.
676 Nonetheless, a total of seven (sub-) watersheds, located in two different geological provinces of
677 southeastern Canada, were considered in this study, which represents an excellent starting point
678 to draw conclusions on how wetland characteristics (parameters) affect stream flows.
679 Alternatively, multivariate statistical methods such as principal component analyses could help
680 comprehend as well which characteristics of a wetlandscape are the most influential on stream
681 flow. While we are confident about our findings, it is noteworthy they are model specific. Although
682 we report similar results from the few related studies, comparable studies are encouraged to
683 evaluate the model-related variability of wetland parameters sensitivity. Moreover, uncertainty
684 associated with input data such as land cover (including wetland mapping) and hydrometric data,
685 model structure and calibration method influence simulated stream flows and wetlands outflows.
686 Although we achieved good calibration performances of the general parameters of HYDROTEL
687 (Table 1), our sensitivity analysis focused on a unique representation of each watershed and a
688 single calibration solution. That being mentioned, we did not account for the uncertainty associated
689 with the input data because this would have required replicating computationally-intensive work.
690 Although we believe this would be relevant as a future step, this was beyond the scope of this
691 paper.

692 **5. Conclusion**

693 In this study, we investigated the spatio-temporal variability of wetland parameter sensitivities
694 using an experimental design for different configurations and locations of wetlandscapes. Our
695 findings emphasize the importance of the geometric parameters on outflows of wetlands at both
696 the hillslope/HEW scale and the watershed scale. The GSA results confirmed that the spatial
697 configuration of wetlands has an effect at the wetland and watershed scales (as previously
698 discussed by Blanchette et al., 2022), which seems mainly driven by the ratio between isolated
699 and riparian wetland surface areas (e.g., wetlandscapes dominated by IWs display higher
700 sensitivity indices for their parameters). Our results also depict a higher sensitivity for IWs located
701 upstream and for RWs located downstream. Finally, we recognize a strong temporal variability, in
702 relation with the various processes dominating the hydrological budget of wetlands, from daily to
703 seasonal time scales. These outcomes can assist model diagnosis and quantitatively investigate
704 the rankings of hydrological processes occurring in wetlands for a given period of the year or
705 specific meteorological events. Although the temporal variability was expected, it is, to our
706 knowledge, the first time a time-varying GSA is performed on the wetland modules of a semi-
707 distributed hydrological model. Knowing that seasonal hydrological processes highly affect
708 wetlands, accounting for this temporal variability is essential to further understand the complexity
709 of model behavior. Our findings will help design field studies where wetland parameters are
710 monitored more intensely during their peak sensitivities. For example, water level monitoring could

711 focus on the spring snowmelt season to provide a better estimation of *WETDMAX*. It is rather
 712 important to notice that our study also contributed to enhance modeling practices as it
 713 demonstrated that the parameter *KSATBK* should be set for RW for lack of sensitivity. All results
 714 will prove useful for land management practices and ever-growing wetland conservation programs
 715 that require the identification of high-value wetlands.

716 **6. Funding**

717 This research was supported by the Fonds de recherche du Québec – Nature et technologies
 718 [204510, 2018-2021], Natural Sciences and Engineering Research of Canada Discovery Program
 719 (grant to A.N.R.), and by the MITACS Accelerate program, the Ouranos consortium (project
 720 554030) via the Quebec government 2013-2020 action plan on climate change, the watershed
 721 organization of the study region (OBV de la Capitale), and Quebec City. MITACS grants were
 722 attributed to M.B.

723 Computations were made on supercomputers Beluga and Narval, managed by Calcul Québec
 724 and the Digital Research Alliance of Canada. The operation of these supercomputers is funded
 725 by the Canada Foundation for Innovation (CFI), Ministère de l'Économie et de l'Innovation du
 726 Québec (MEI) and les Fonds de recherche du Québec (FRQ).

727 **7. Acknowledgments**

728 We would like to thank the two anonymous reviewers for their constructive comments, which
 729 significantly improved the article. We also acknowledge Québec City for providing rain gauge and
 730 water withdrawal data.

731 **8. References**

- 732 Agence des forêts privées du Québec 03, 2001. Plan de protection et de mise en valeur du
 733 territoire (PPMV). 190 p.
- 734 Agence Forestière des Bois-Francs, 2015. Plan de protection et de mise en valeur des forêts
 735 privées du Centre-du-Québec, Tome 1 - Portrait du territoire. 159 p.
- 736 Asadzadeh, M., Tolson, B.A., 2009. A new multi-objective algorithm, pareto archived DDS,
 737 Proceedings of the 11th Annual Conference Companion on Genetic and Evolutionary
 738 Computation Conference: Late Breaking Papers. Association for Computing Machinery,
 739 Montreal, Québec, Canada, pp. 1963–1966. <https://doi.org/10.1145/1570256.1570259>.
- 740 Bajracharya, A., Awoye, H., Stadnyk, T., Asadzadeh, M., 2020. Time Variant Sensitivity Analysis
 741 of Hydrological Model Parameters in a Cold Region Using Flow Signatures. *Water*. 12(4),
 742 1-24. <https://doi.org/ARTN 96110.3390/w12040961>.
- 743 Beck, H.E., Zimmermann, N.E., McVicar, T.R., Vergopolan, N., Berg, A., Wood, E.F., 2018.
 744 Present and future Koppen-Geiger climate classification maps at 1-km resolution. *Sci Data*.
 745 5(180214). <https://doi.org/10.1038/sdata.2018.214>.
- 746 Ben Nasr, I., 2014. Incertitudes sur les débits simulés par le modèle HYDROTEL attribuables aux
 747 incertitudes sur les paramètres - Application au bassin de la rivière Beauvillage, Québec,
 748 Canada, 78 pp.

- 749 Blanchette, M., Rousseau, A.N., Savary, S., Foulon, E., 2022. Are spatial distribution and
750 aggregation of wetlands reliable indicators of stream flow mitigation? *J. Hydrol.* 608.
751 <https://doi.org/10.1016/j.jhydrol.2022.127646>.
- 752 Bouda, M., Rousseau, A.N., Gumiere, S.J., Gagnon, P., Konan, B., Moussa, R., 2014.
753 Implementation of an automatic calibration procedure for HYDROTEL based on prior OAT
754 sensitivity and complementary identifiability analysis. *Hydrol. Processes.* 28(12), 3947-
755 3961. <https://doi.org/10.1002/hyp.9882>.
- 756 Bouda, M., Rousseau, A.N., Konan, B., Gagnon, P., Gumiere, S.J., 2012. Bayesian Uncertainty
757 Analysis of the Distributed Hydrological Model HYDROTEL. *Journal of Hydrologic*
758 *Engineering.* 17(9), 1021-1032. [https://doi.org/10.1061/\(asce\)he.1943-5584.0000550](https://doi.org/10.1061/(asce)he.1943-5584.0000550).
- 759 Brodeur, C., Lewis, F., Huet-Alegre, E., Ksouri, Y., Leclerc, M.-C., Viens, D., 2009. Portrait du
760 bassin de la rivière Saint-Charles, 2e édition. . Conseil de bassin de la rivière Saint-
761 Charles., pp. 216.
- 762 [dataset] Canards Illimités Canada, Ministère de l'Environnement et Lutte contre les changements
763 climatiques, 2020. Cartographie détaillée des milieux humides des secteurs habités du
764 sud du Québec – Données du projet global, Québec (Québec).
765 <https://www.donneesquebec.ca/recherche/fr/dataset/milieux-humides-du-quebec>.
- 766 Cukier, R.I., Fortuin, C.M., Shuler, K.E., Petschek, A.G., Schaibly, J.H., 1973. Study of the
767 sensitivity of coupled reaction systems to uncertainties in rate coefficients. . I. Theory *J.*
768 *Chem. Phys.* . 59(8), 3873-3878. <https://doi.org/10.1063/1.1680571>.
- 769 Environmental Systems Research Institute (ESRI), ArcGIS for Desktop, Redlands, California,
770 USA. <https://www.esri.com/>.
- 771 Evenson, G.R., Golden, H.E., Lane, C.R., McLaughlin, D.L., D'Amico, E., 2018. Depressional
772 wetlands affect watershed hydrological, biogeochemical, and ecological functions. *Ecol*
773 *Appl.* 28(4), 953-966. <https://doi.org/10.1002/eap.1701>.
- 774 Fortin, J.-P., Turcotte, R., Massicotte, S., Moussa, R., Fitzback, J., Villeneuve, J.-P., 2001.
775 Distributed Watershed Model Compatible with Remote Sensing and GIS Data. I:
776 Description of Model. *Journal of Hydrologic Engineering.* 6(2), 91-99.
777 [https://doi.org/10.1061/\(asce\)1084-0699\(2001\)6:2\(91\)](https://doi.org/10.1061/(asce)1084-0699(2001)6:2(91)).
- 778 Fossey, M., Rousseau, A.N., 2016a. Assessing the long-term hydrological services provided by
779 wetlands under changing climate conditions: A case study approach of a Canadian
780 watershed. *J. Hydrol.* 541, 1287-1302. <https://doi.org/10.1016/j.jhydrol.2016.08.032>.
- 781 Fossey, M., Rousseau, A.N., 2016b. Can isolated and riparian wetlands mitigate the impact of
782 climate change on watershed hydrology? A case study approach. *J Environ Manage.*
783 184(Pt 2), 327-339. <https://doi.org/10.1016/j.jenvman.2016.09.043>.
- 784 Fossey, M., Rousseau, A.N., Bensalma, F., Savary, S., Royer, A., 2015. Integrating isolated and
785 riparian wetland modules in the PHYSITEL/HYDROTEL modelling platform: model
786 performance and diagnosis. *Hydrol. Processes.* 29(22), 4683-4702.
787 <https://doi.org/10.1002/hyp.10534>.

- 788 Fossey, M., Rousseau, A.N., Savary, S., 2016. Assessment of the impact of spatio-temporal
789 attributes of wetlands on stream flows using a hydrological modelling framework: a
790 theoretical case study of a watershed under temperate climatic conditions. *Hydrol.*
791 *Processes.* 30(11), 1768-1781. <https://doi.org/10.1002/hyp.10750>.
- 792 Gerardin, V., McKenney, D., 2001. Une classification climatique du Québec à partir de modèles
793 de distribution spatiale de données climatiques mensuelles : vers une définition des
794 bioclimats du Québec., Direction du patrimoine écologique et du développement durable,
795 ministère de l'Environnement, Québec. 48 p.
796 <http://www.mddelcc.gouv.qc.ca/changements/classification/model-clima.pdf>.
- 797 Goyette, J.-O., Savary, S., Blanchette, M., Rousseau, A.N., Pellerin, S., Poulin, M., 2022. Setting
798 targets for wetland restoration to mitigate climate change effects on watershed hydrology.
799 *Environmental Management*.
- 800 Gupta, H.V., Kling, H., Yilmaz, K.K., Martinez, G.F., 2009. Decomposition of the mean squared
801 error and NSE performance criteria: Implications for improving hydrological modelling. *J.*
802 *Hydrol.* 377(1-2), 80-91. <https://doi.org/10.1016/j.jhydrol.2009.08.003>.
- 803 Gupta, H.V., Razavi, S., 2018. Revisiting the Basis of Sensitivity Analysis for Dynamical Earth
804 System Models. *Water Resour. Res.* 54(11), 8692-8717.
805 <https://doi.org/10.1029/2018wr022668>.
- 806 Hallouin, T., 2021. HydroEval: Streamflow Simulations Evaluator. Zenodo.
807 <https://doi.org/10.5281/zenodo.2591217>.
- 808 Hughes, R.M., Kaufmann, P.R., Weber, M.H., 2011. National and regional comparisons between
809 Strahler order and stream size. *Journal of the North American Benthological Society.* 30(1),
810 103-121. <https://doi.org/10.1899/09-174.1>.
- 811 Iman, R., Helton, J., 1988. An investigation of uncertainty and sensitivity analysis techniques for
812 computer models. *Risk Anal.* 8, 71-90.
- 813 Jones, C.N., Evenson, G.R., McLaughlin, D.L., Vanderhoof, M.K., Lang, M.W., McCarty, G.W.,
814 Golden, H.E., Lane, C.R., Alexander, L.C., 2018. Estimating restorable wetland water
815 storage at landscape scales. *Hydrol Process.* 32(2), 305-313.
816 <https://doi.org/10.1002/hyp.11405>.
- 817 Korgaonkar, Y., Meles, M.B., Guertin, D.P., Goodrich, D.C., Unkrich, C., 2020. Global sensitivity
818 analysis of KINEROS2 hydrologic model parameters representing green infrastructure
819 using the STAR-VARS framework. *Environ. Model. Software.* 132.
820 <https://doi.org/10.1016/j.envsoft.2020.104814>.
- 821 Litynski, J., 1988. Climat du Québec d'après la classification numérique, pp. Carte de format 100
822 x 130 cm.
- 823 Liu, Y.B., Yang, W.H., Wang, X.X., 2008. Development of a SWAT extension module to simulate
824 riparian wetland hydrologic processes at a watershed scale. *Hydrol. Processes.* 22(16),
825 2901-2915. <https://doi.org/10.1002/hyp.6874>.
- 826 Mailhot, A., Villeneuve, J.P., 2003. Mean-value second-order uncertainty analysis method:
827 application to water quality modelling. *Adv. Water Resour.* 26(5), 491-499.

- 828 Matott, S.L., 2017. OSTRICH – An Optimization Software Toolkit for Research Involving
829 Computational Heuristics Documentation and User's Guide Version 17.12.19, University
830 at Buffalo Center for Computational Research. 79 p.
831 <http://www.civil.uwaterloo.ca/envmodelling/Ostrich.html>.
- 832 McLaughlin, D.L., Kaplan, D.A., Cohen, M.J., 2014. A significant nexus: Geographically isolated
833 wetlands influence landscape hydrology. *Water Resour. Res.* 50(9), 7153-7166.
834 <https://doi.org/10.1002/2013wr015002>.
- 835 Medina, Y., Muñoz, E., 2020. A Simple Time-Varying Sensitivity Analysis (TVSA) for Assessment
836 of Temporal Variability of Hydrological Processes. *Water*. 12(9), 2463.
- 837 [dataset] Ministère de l'Environnement et la Lutte contre les Changements Climatiques, 2021.
838 Daily hydrometric data.
839 https://www.cehq.gouv.qc.ca/hydrometrie/historique_donnees/index.asp.
- 840 Morin, P., Boulanger, F., 2005. Portrait de l'environnement du bassin versant de la rivière
841 Bécancour. Rapport produit par Envir-Action pour le Groupe de concertation du bassin de
842 la rivière Bécancour (GROBEC), Plessisville, Québec, Canada, pp. 197.
- 843 Morris, M.D., 1991. Factorial Sampling Plans for Preliminary Computational Experiments.
844 *Technometrics*. 33(2), 161-174. <https://doi.org/10.2307/1269043>.
- 845 [dataset] Natural Resources Canada, 2013. Digital elevation model of Canada.
- 846 Noël, P., Rousseau, A.N., Paniconi, C., Nadeau, D.F., 2014. Algorithm for Delineating and
847 Extracting Hillslopes and Hillslope Width Functions from Gridded Elevation Data. *Journal*
848 *of Hydrologic Engineering*. 19(2), 366-374. [https://doi.org/10.1061/\(asce\)he.1943-5584.0000783](https://doi.org/10.1061/(asce)he.1943-5584.0000783).
- 850 Oudin, L., Andréassian, V., Mathevet, T., Perrin, C., Michel, C., 2006. Dynamic averaging of
851 rainfall-runoff model simulations from complementary model parameterizations. *Water*
852 *Resour. Res.* 42(7). <https://doi.org/10.1029/2005wr004636>.
- 853 Pianosi, F., Wagener, T., 2015. A simple and efficient method for global sensitivity analysis based
854 on cumulative distribution functions. *Environ. Model. Softw.* 67, 1-11.
855 <https://doi.org/10.1016/j.envsoft.2015.01.004>.
- 856 Pianosi, F., Wagener, T., 2016. Understanding the time-varying importance of different uncertainty
857 sources in hydrological modelling using global sensitivity analysis. *Hydrol. Processes*.
858 30(22), 3991-4003. <https://doi.org/10.1002/hyp.10968>.
- 859 R Core Team, 2020. R: A language and environment for statistical computing. R Foundation for
860 Statistical Computing, Vienna, Austria. <https://www.R-project.org/>.
- 861 Rahman, M.M., Thompson, J.R., Flower, R.J., 2016. An enhanced SWAT wetland module to
862 quantify hydraulic interactions between riparian depressional wetlands, rivers and aquifers.
863 *Environ. Model. Software*. 84, 263-289. <https://doi.org/10.1016/j.envsoft.2016.07.003>.
- 864 Razavi, S., Gupta, H.V., 2016a. A new framework for comprehensive, robust, and efficient global
865 sensitivity analysis: 1. Theory. *Water Resour. Res.* 52(1), 440-455.
866 <https://doi.org/10.1002/2015wr017559>.

- 867 Razavi, S., Gupta, H.V., 2016b. A new framework for comprehensive, robust, and efficient global
 868 sensitivity analysis: 2. Application. *Water Resour. Res.* 52(1), 423-439.
 869 <https://doi.org/10.1002/2015wr017558>.
- 870 Razavi, S., Gupta, H.V., 2019. A multi-method Generalized Global Sensitivity Matrix approach to
 871 accounting for the dynamical nature of earth and environmental systems models. *Environ.*
 872 *Model. Software.* 114, 1-11. <https://doi.org/10.1016/j.envsoft.2018.12.002>.
- 873 Razavi, S., Jakeman, A., Saltelli, A., Prieur, C., Iooss, B., Borgonovo, E., Plischke, E., Lo Piano,
 874 S., Iwanaga, T., Becker, W., Tarantola, S., Guillaume, J.H.A., Jakeman, J., Gupta, H.,
 875 Melillo, N., Rabitti, G., Chabridon, V., Duan, Q., Sun, X., Smith, S., Sheikholeslami, R.,
 876 Hosseini, N., Asadzadeh, M., Puy, A., Kucherenko, S., Maier, H.R., 2021. The Future of
 877 Sensitivity Analysis: An essential discipline for systems modeling and policy support.
 878 *Environ. Model. Software.* 137. <https://doi.org/10.1016/j.envsoft.2020.104954>.
- 879 Razavi, S., Sheikholeslami, R., Gupta, H.V., Haghnegahdar, A., 2019. VARS-TOOL: A toolbox for
 880 comprehensive, efficient, and robust sensitivity and uncertainty analysis. *Environ. Model.*
 881 *Software.* 112, 95-107. <https://doi.org/10.1016/j.envsoft.2018.10.005>.
- 882 Reusser, D.E., Buytaert, W., Zehe, E., 2011. Temporal dynamics of model parameter sensitivity
 883 for computationally expensive models with the Fourier amplitude sensitivity test. *Water*
 884 *Resour. Res.* 47(7). <https://doi.org/10.1029/2010wr009947>.
- 885 Rousseau, A.N., Fortin, J.P., Turcotte, R., Royer, A., Savary, S., Quévy, F., Noël, P., Paniconi, C.,
 886 2011. PHYSITEL, a specialized GIS for supporting the implementation of distributed
 887 hydrological models. *Water News - Official Magazine of the Canadian Water Resources*
 888 *Association.* 31(1), 18-20.
- 889 Rousseau, A.N., Savary, S., Bazinet, M.-L., 2022. Flood water storage using active and passive
 890 approaches - Assessing flood control attributes of wetlands and riparian agricultural land
 891 in the Lake Champlain-Richelieu River watershed. A Report to the International Lake
 892 Champlain - Richelieu River Study Board. 92 p.
- 893 Saltelli, A., Tarantola, S., Campolongo, F., Ratto, M., 2004. *Sensitivity Analysis in Practice*, 232
 894 pp.
- 895 Singh, J., Knapp, H.V., Arnold, J.G., Demissie, M., 2005. Hydrologic modeling of the Iroquois river
 896 watershed using HSPF and SWAT. *J. Am. Water Resour. Assoc.*(2), 343–360.
 897 <https://doi.org/10.1111/j.1752-1688.2005.tb03740.x>.
- 898 Sobol, I.M., 1993. Sensitivity estimates for nonlinear mathematical models. *Math. Model. Comput.*
 899 *Exp.* . 1(4), 407-414. <https://doi.org/1061-7590/93/04407-008>.
- 900 [dataset] Soil Landscapes of Canada Working Group, 2010. *Soil Landscapes of Canada v3.2*.
- 901 Strahler, A.N., 1957. Quantitative analysis of watershed geomorphology. *Transactions, American*
 902 *Geophysical Union.* 38(6), 913-920. <https://doi.org/10.1029/TR038i006p00913>.
- 903 Tolson, B.A., Sharma, V., Swayne, D.A., 2014. Parallel Implementations of the Dynamically
 904 Dimensioned Search (DDS) Algorithm, *Environmental Software Systems*, Prague, Czech
 905 Republic, pp. 573-582. <https://doi.org/10.13140/2.1.3773.6001>.

- 906 Turcotte, R., Fortin, J.P., Rousseau, A.N., Massicotte, S., Villeneuve, J.P., 2001. Determination of
907 the drainage structure of a watershed using a digital elevation model and a digital river and
908 lake network. *J. Hydrol.* 240(3-4), 225-242. [https://doi.org/10.1016/s0022-1694\(00\)00342-](https://doi.org/10.1016/s0022-1694(00)00342-5)
909 [5](https://doi.org/10.1016/s0022-1694(00)00342-5).
- 910 Turcotte, R., Fortin, L.G., Fortin, V., Fortin, J.P., Villeneuve, J.P., 2007. Operational analysis of
911 the spatial distribution and the temporal evolution of the snowpack water equivalent in
912 southern Québec, Canada. *Hydrology Research.* 38(3), 211-234.
913 <https://doi.org/10.2166/nh.2007.009>.
- 914 Turcotte, R., Rousseau, A.N., Fortin, J.-P., Villeneuve, J.-P., 2003. A Process-Oriented, Multiple-
915 Objective Calibration Strategy Accounting for Model Structure, in: Duan, Q., Gupta, H.V.,
916 Sorooshian, S., Rousseau, A.N., Turcotte, R. (Eds.), *Calibration of Watershed Models*.
917 American Geophysical Union, Washington, D. C., pp. 345.
918 <https://doi.org/10.1002/9781118665671.ch11>.
- 919 Wang, S., Yang, Y., Luo, Y., Rivera, A., 2013. Spatial and seasonal variations in
920 evapotranspiration over Canada's landmass. *Hydrol. Earth Syst. Sci.* 17(9), 3561-3575.
921 <https://doi.org/10.5194/hess-17-3561-2013>.
- 922 Wang, X., Yang, W., Melesse, A.M., 2008. Using Hydrologic Equivalent Wetland Concept Within
923 SWAT to Estimate Streamflow in Watersheds with Numerous Wetlands. *Transactions of*
924 *the ASABE.* 51(1), 55-72. <https://doi.org/10.13031/2013.24227>.
- 925 Wu, Y., Sun, J., Jun Xu, Y., Zhang, G., Liu, T., 2022. Projection of future hydrometeorological
926 extremes and wetland flood mitigation services with different global warming levels: A case
927 study in the Nenjiang river basin. *Ecological Indicators.* 140.
928 <https://doi.org/10.1016/j.ecolind.2022.108987>.
- 929 Wu, Y., Zhang, G., Rousseau, A.N., Xu, Y.J., 2020a. Quantifying streamflow regulation services
930 of wetlands with an emphasis on quickflow and baseflow responses in the Upper Nenjiang
931 River Basin, Northeast China. *J. Hydrol.* 583.
932 <https://doi.org/10.1016/j.jhydrol.2020.124565>.
- 933 Wu, Y., Zhang, G., Rousseau, A.N., Xu, Y.J., Foulon, É., 2020b. On how wetlands can provide
934 flood resilience in a large river basin: A case study in Nenjiang river Basin, China. *J. Hydrol.*
935 587. <https://doi.org/10.1016/j.jhydrol.2020.125012>.
- 936 Wu, Y.F., Zhang, G.X., Xu, Y.J., Rousseau, A.N., 2021. River Damming Reduces Wetland
937 Function in Regulating Flow. *J Water Res Plan Man.* 147(10).
938 [https://doi.org/10.1061/\(Asce\)Wr.1943-5452.0001434](https://doi.org/10.1061/(Asce)Wr.1943-5452.0001434).
- 939 Xi, Y., Peng, S., Ducharme, A., Ciais, P., Gumbricht, T., Jimenez, C., Poulter, B., Prigent, C., Qiu,
940 C., Saunois, M., Zhang, Z., 2022. Gridded maps of wetlands dynamics over mid-low
941 latitudes for 1980-2020 based on TOPMODEL. *Sci Data.* 9(1), 347.
942 <https://doi.org/10.1038/s41597-022-01460-w>.
- 943 Yapo, P.O., Gupta, H.V., Sorooshian, S., 1996. Automatic calibration of conceptual rainfall-runoff
944 models: sensitivity to calibration data. *J. Hydrol.* 181(1-4), 23-48.
945 [https://doi.org/10.1016/0022-1694\(95\)02918-4](https://doi.org/10.1016/0022-1694(95)02918-4).

946 Zambrano-Bigiarini, M., 2020. hydroGOF: Goodness-of-fit functions for comparison of simulated
947 and observed hydrological time series. <https://doi.org/10.5281/zenodo.839854>.

948

949 **Abstract**

950 Hydrological models offer the opportunity to evaluate wetland conservation networks as nature-
951 based solutions to mitigate hydrological extremes. To optimize the replication of a hydrological
952 model response (i.e., stream flows), the models rely on input data (land cover, hydrographic
953 network, soil types, topography, meteorological data) and parameters. However, the effect of
954 parametric uncertainty on the simulated variables and the spatio-temporal variability of this
955 sensitivity are insufficiently documented. This study presents an application of the novel global
956 sensitivity analysis method, the Variogram Analysis of Response Surface, to the isolated and
957 riparian wetland modules of HYDROTEL, a semi-distributed, process-based, deterministic model,
958 on two watersheds located in the province of Quebec, Canada. The analysis accounted for: (i) the
959 spatial variability by assessing the sensitivity at various locations in the watersheds and by
960 compiling sensitivity indices for wetland networks discretized following the Strahler order
961 classification which quantifies the structure of hydrographic networks and (ii) the temporal
962 variability of the sensitivity using the Generalized Global Sensitivity Matrix. The results indicate
963 that the parameters defining the geometry of wetlands (area, depth) are the most sensitive for
964 both isolated and riparian wetlands, and for all Strahler orders. The temporal assessment of
965 sensitivity highlights the seasonal controlling processes, including a peaking sensitivity of the
966 maximum water depth in wetlands during spring snowmelt, whereas the sensitivity of the
967 evapotranspiration parameter increases during summer, but is null during winter. Results also
968 indicate that the parameters of the isolated modules are more sensitive for wetlands located on
969 lower stream order (upstream/headwaters) while those of the riparian modules display a greater
970 sensitivity when wetlands are located on higher Strahler orders (downstream/main channel).
971 These findings deepen our understanding of the impact of wetland features on stream flows and
972 provide guidelines to plan future data acquisition campaigns in wetlandscapes.

973

974 **Keywords**

975 HYDROTEL, hydroconnectivity, time-varying sensitivity analysis, Variogram Analysis of Response
976 Surface, field data acquisition, Strahler order

977

978 **Marianne Blanchette:** Conceptualization, Methodology, Software, Writing- Original draft, Writing-
979 Reviewing and Editing, Visualization, Formal Analysis, Investigation. **Étienne Foulon:** Conceptualization,
980 Methodology, Software, Writing – Reviewing and Editing. **Alain N. Rousseau:** Conceptualization,
981 Methodology, Writing – Reviewing and Editing, Supervision

982

983 **Highlights**

- 984
- 985 • Geometry dominates the sensitivity at both the wetland and the watershed scale.
 - 986 • Hydroconnectivity strongly influences the sensitivity among wetland parameters.
 - The sensitivity of wetland parameters display a high temporal variability.

987 • Sensitivity analysis can support site selection and timing for field monitoring.

988

Journal Pre-proofs